FED-Vol. 176, Bubble Noise and Cavitation Erosion
in Fluid Systems
ASME 1993

EROSION VIBRATORY FINGERPRINT OF LEADING EDGE CAVITATION OF A NACA PROFILE AND OF A FRANCIS MODEL AND PROTOTYPE HYDROTURBINE

Paul Bourdon
Mechanical Research
Hydro-Québec – IREQ
Varennes, Québec, Canada

Raynald Simoneau
Materials Technology Res.
Hydro-Québec – IREQ
Varennes, Québec, Canada

François Avellan
IMHEF-EPFL
Lausanne, Vaud, Switzerland

ABSTRACT

This paper summarizes the findings of CEA project No 307 G 657 entitled "Hydraulic Turbine Cavitation Pitting Detection by Monitoring Runner Vibration." The project was centered on the detection of leading edge cavitation, the main cause of erosion damage on Francis turbines. Based on a damage model proposed by EPFL of Lausanne [1-2] and verified by EPFL and IREQ [3], the vibratory signature of erosive cavitation was first sought on a bi-dimensional NACA 009 profile in a high speed cavitation tunnel and then on the model and the prototype of a Francis turbine design. The main results of these investigations are presented. These show that the damage mechanism observed in the cavitation tunnel appears to also apply to the model and the prototype but its vibratory signature is modified and is determined by overall system flow characteristics that can vary from model to prototype if complete system homology is not maintained. Appropriate measurements on the fixed part of the machine were found to be equivalent to those made on the rotating part.

INTRODUCTION

The specific objective of Canadian Electrical Association project 307 G 657 entitled "Hydraulic Turbine Cavitation Pitting Detection by Monitoring Runner Vibration" was to identify a cavitation pitting fingerprint by comparing the response of suitable detectors mounted centrally in the crown of a turbine runner so that vibration is picked up directly from the metal being eroded to that of accelerometers on the lower guide bearing housing. Measurements at this latter point had shown themselves to be promising in this regard in CEA project 230 G 439, "Cavitation Detection in Model Tests of Hydraulic Turbines" [4]. To achieve this objective, we first attempted to identify the vibratory signature of leading edge erosive cavitation under well controlled laboratory conditions on a bi-dimensional stainless steel NACA 009 profile in the IMHEF high speed cavitation tunnel [5]. With that information in hand we then sought the same signatures on a Francis model in the DEW Hydraulic Laboratory in Lachine, Québec. The model was equipped with both rotating and fixed high frequency accelerometers. And finally, the same signature was again sought on the Francis prototype of the model in the Rapide Blanc powerhouse on the upper St-Maurice River in Québec. Again, fixed and rotating sensors were utilized. We will now proceed to a description of these three phases and their more significant results.

HIGH SPEED CAVITATION TUNNEL INVESTIGATION

The results of this first phase of the project have been presented previously [7] but are summarized here so that a complete project overview can be presented.

Test Set-Up

NACA 009 Profile. A specially machined Stainless Steel NACA 009 profile was equipped with seven DECER [3] titanium electrochemical erosion detectors mounted flush with

the low-pressure surface. The profile was machined with a slanted trailing edge to minimize dynamic forces on it generated by Von Karman eddies at the trailing edge. The hydrofoil with the DECER sensors was mounted in the cavitation tunnel test section [5] as shown in Figure 1.

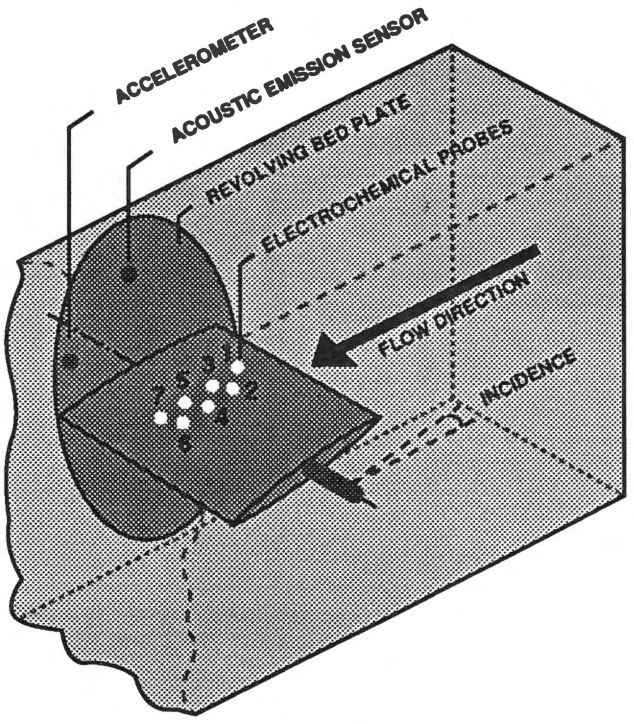

FIGURE 1 NACA PROFILE IN TEST SECTION

Sensors. In addition to the DECER probes, a high frequency accelerometer (Kistler 8616A 1000) with a dynamic range of ± 1000 g and a nominal catalog mounted resonance frequency of 125 kHz and a Physical Acoustics Corporation wide band WD acoustic emission sensor operating in the 100-1000 kHz frequency range were installed on the back of the revolving bed plate into which the profile was imbedded. The sensitive axis of these sensors was parallel to the axis of rotation of the profile. A miniature high frequency force hammer (Dytran 5800 SL) was also utilised to measure the Transmissibility function between the surface of the profile near the DECER probes and the response accelerometer on the back of the bed plate. Hydrodynamic parameters were provided by the tunnel data acquisition sensors and systems [5]. A 35 mm camera photographed the profile in the test section at the beginning and end of each test period. A stroboscopic lamp was utilized to observe the leading edge cavity during test sequences.

Data Acquisition Systems. The data acquisition systems utilized for the DECER and vibration sensors are illustrated in Figure 2. These same systems except for the DECER probe acquisition system were utilized with slight modifications in the number of sensors and bandwidths used for the model and prototype tests.

Hydrodynamic Test Conditions. A total of 55 sets of hydrodynamic test conditions were explored. Blade tilt angles varied between 2.5 and 4.5 degrees, sigma values between .7 and 1.4 and water velocities between 20 and 42.5 m/sec. The combinations of tilt angles, sigma values and water velocities were chosen so that leading edge cavities could be made to cover progressively greater lengths of the profile so that areas of maximum erosion could be identified in relation to the location of the DECER probes on the profile and to the intensity of the measured profile vibrations as a result of the impact forces generated by the imploding cavitation vortices. Test conditions were chosen to provide cavity lengths such that the vortices would implode on the profile and not in the flow behind it.

Program Results

Transient Vortex Shedding Frequency. Previous research at IMHEF had suggested [1-2] that cavitation damage associated with leading edge cavitation was due to the implosion of U shaped transient vortices downstream of the leading edge cavity. Such a damage model was also strengthened by systematic visualizations on models and actual damage localization on the corresponding prototypes [2]. Although the rate of production of these U shaped vortices visible in Figure 3 had been evaluated by laser Doppler anemometry, their rate of implosion on the NACA profile had to be confirmed. This was achieved by frequency analyzing the amplitude envelope of high frequency acceleration of the profile in the 15 to 35 kHz frequency band and correlating the main modulation frequency for each set of test conditions with the ratio of the mean flow velocity to the observed mean leading edge cavity length. The results of that correlation appears in Figure 4. It can be seen that the implosion frequency is governed by a very well defined Strouhal relation. That frequency corresponds to the pulsation frequency of the leading edge cavity observed previously with laser Doppler anemometry [1].

Erosion Damage Localization. With the distribution of DECER probes on the profile it was possible to determine the area of maximum erosion in relation to the average leading edge cavity length. As had been observed previously [3] and in accord with the proposed leading edge cavitation damage mechanism [1-3], the area of maximum erosion was found to be in the closure region of the leading edge cavity. An illustration of this can be found in Figure 5 which shows the individual DECER probe erosion rates versus their position X along the profile chord length L in relation to the length of the leading edge cavity given by the length of the arrow for each case. Since the DECER probes cover only a portion of the complete profile area and in consideration of the localized character of the distribution of observed erosion rates, the average erosion rate

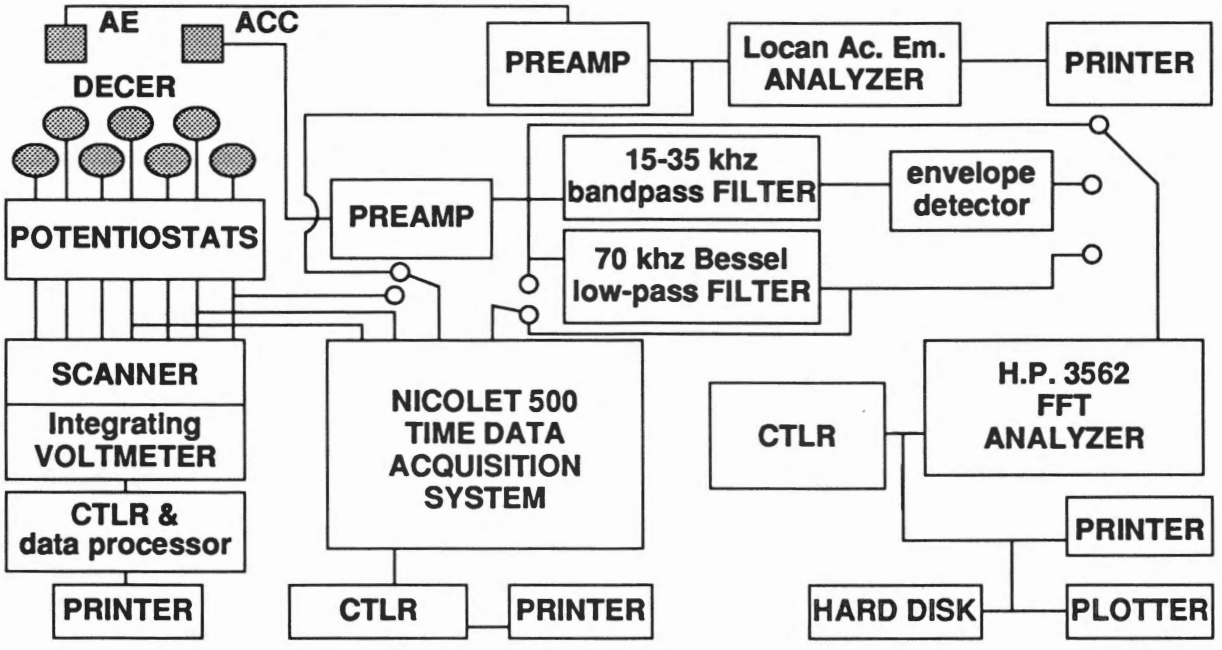

FIGURE 2 DECER AND VIBRATION DATA ACQUISITION SYSTEMS

FIGURE 3 U SHAPED TRANSIENT VORTICES WITH LEADING EDGE CAVITATION

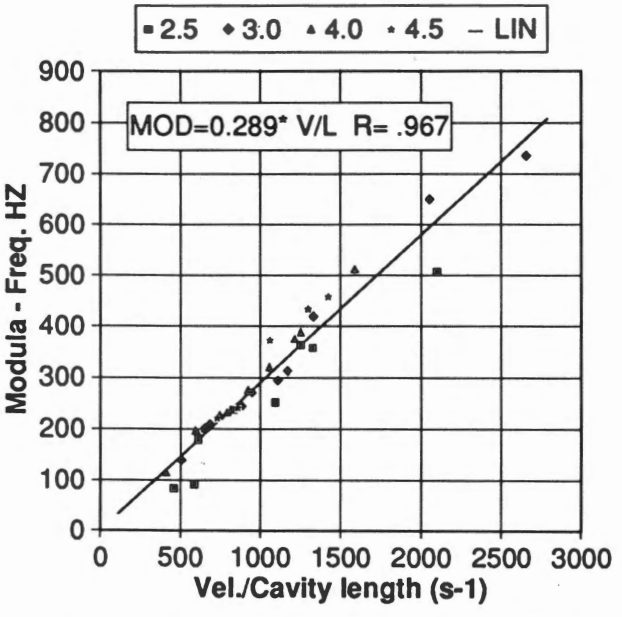

FIGURE 4 STROUHAL RELATION GOVERNING IMPLOSION FREQUENCIES

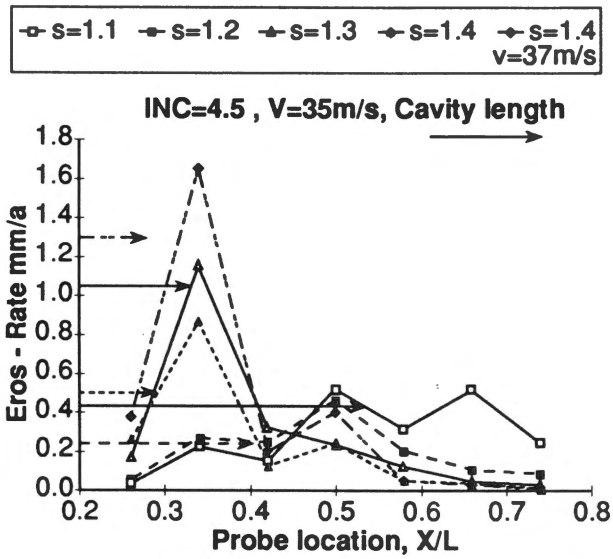

FIGURE 5 LOCALIZED EROSION RATE IN RELATION TO CAVITY LENGTH ON PROFILE

over the seven probes (Σ of localized erosion rates/number of probes) has been considered as indicative of the average erosion rate over the complete profile.

Correlation Between Acceleration and Erosion Rate.

In the correlation studies that were performed between measured vibratory parameters and average erosion rate, the parameter to which the erosion rate was best linearly related was the mean square value of acceleration in the 15 to 35 kHz frequency band. The observed relation is illustrated in Figure 6. The 15 to 35 kHz frequency band was retained for measurement purposes as a compromise in consideration of the following factors:

- when measuring the effects of cavitation which excites a very broad spectrum of frequencies(into the hundreds and even thousands of kHz), it is wishful to measure in as high a frequency band as possible to avoid contamination of the signal by low frequency noise from other mechanical or hydraulic sources.
- however, since available accelerometers with adequate sensitivity are limited in flat frequency response to an upper frequency of about 30 to 35 kHz, it is desirable to use this frequency band so that absolute acceleration measurements can be performed with minimal error caused by the accelerometer direct and transverse mounted resonances which are generally excited by the cavitation impacts.
- a 20 kHz bandwidth provides a reasonable signal level to improve the signal to electronic noise ratio in the instrumentation.
- this frequency range allows calibration with a miniature impact hammer of the transmissibility function between the profile surface and the accelerometer mounting location.

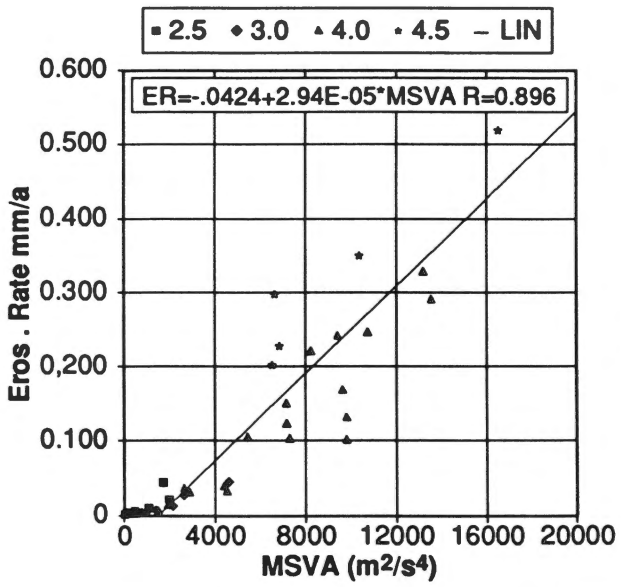

FIGURE 6 EROSION RATE VS THE MSV OF ACCELERATION IN THE 15 TO 35 kHZ FREQUENCY BAND

Only the points (29) showing erosion rates of .01 mm/annum or more of titanium were retained in the curve fitting exercise because of the detection threshold of the DECER probes which was typically between 0.001 and 0.005 mm/a with slight fluctuations about these values during low level cavitation test conditions. The low level erosion points were excluded from the data to minimize errors and therefore the curve on the graph represents more correctly the situation when meaningful erosion levels were measured. It should be noted that excellent linear correlations were also obtained in later experimentation between cavitation erosion rates and the MSV of acceleration in selected frequency bands in both vibratory and jet cavitation erosion facilities [6].

A possible explanation for this linear relation rests on the following considerations. Cavitation erosion is proportional to the power in the cavitating flow which is effectively used on the turbine to produce the erosion. This power is expressed as

$$P_{er} = \frac{dW}{dt} \tag{1}$$

where W is work and t is time.

W is expressed by $$W = \int F\,dx \tag{2}$$

where F is an applied force and x its displacement.

Substituting (2) in (1),

$$P_{er} = \frac{d}{dt}\int F\,dx \tag{3}$$

TABLE 1
LINEAR CURVE FIT CORRELATION COEFFICIENTS

	Parameter								
	MSVA	MSVV1	MSVV2	MSVF1	MSVF2	MSVM1	MSVM2	$\Sigma A_i N_i$	C.FACT.
Correlation coefficient	.901	.803	.341	.797	.649	.840	.819	.852	.248

For a single degree of freedom mass, spring, viscous damper system, F is equal to the system reaction forces according to

$$F = m\ddot{x} + c\dot{x} + kx \tag{4}$$

where m is mass, c is viscous damping coefficient, k is spring stiffness, $\ddot{x}$ is acceleration, $\dot{x}$ is velocity and x, displacement. Introducing (4) in (3),

$$P_{er} = \frac{d}{dt}\int (m\ddot{x} + c\dot{x} + kx)dx \tag{5}$$

and considering that $dx = \frac{dx}{dt}dt = \dot{x}\,dt$, then

$$P_{er} = \frac{d}{dt}\int (m\ddot{x} + c\dot{x} + kx)\,\dot{x}\,dt \tag{6}$$

and

$$P_{er} = m\ddot{x}\,\dot{x} + c(\dot{x})^2 + k\,x\,\dot{x} \tag{7}$$

If we consider this power for one vibration mode of the structure at a frequency ω_1, and transform velocity and displacement terms into equivalent acceleration terms, then

$$P_{er_{\omega_1}} = \frac{m(\ddot{x})^2}{\omega_1} + \frac{c(\ddot{x})^2}{\omega_1^2} + \frac{k(\ddot{x})^2}{\omega_1^3} \tag{8}$$

Since mechanical power is proportional to a parameter including a squared displacement term, the erosive power should also be proportional to a parameter such as the square of the acceleration $\ddot{x}\left(\frac{m^2}{\sec^4}\right)$ at a single frequency ω_1. When a structure is linear and a frequency bandwidth is considered, the contributions of each of the excited modes of the structure to the acceleration in that bandwidth can be identified by Fourier analysis of the acceleration signal. Then, by superposition, the total erosion power in that bandwidth becomes proportional to the sum of the squares of the acceleration for all excited modes at each frequency in that bandwidth. That is evaluated by taking the MSV of acceleration in that frequency band. If a high frequency band is considered, the last 2 terms in equation (8) corresponding to viscous and elastic reaction forces become increasingly less significant as the frequency increases particularly above the resonance frequency of each mode. Only the purely inertial term remains which is proportional to the square of the acceleration. On the basis of this model, the MSV of acceleration in a high frequency band would become a logical parameter to follow for the monitoring of erosive cavitation. The results obtained here and in reference [6] tend to support this model.

The parameters that were evaluated as possible cavitation erosion monitors on the profile in the high speed cavitation tunnel follow:

MSVA : The mean square value (MSV) of acceleration in the 15 to 35 kHz frequency band.

MSVV1 : The MSV of velocity in the 15 to 30 kHz frequency band.

MSVV2 : The MSV of velocity in the 62.5 to 3000 Hz frequency band.

MSVF1 : The MSV of inferred forces on the profile in the 15 to 30 kHz frequency band.

MSVF2 : The MSV of inferred forces on the profile in the 62.5 to 3000 Hz frequency band.

MSVM1: The MSV of amplitude modulation in the 25 to 3000 Hz frequency band of the high frequency acceleration in the 15 to 35 kHz frequency band.

MSVM2: The MSV of amplitude modulation in the 3 to 5 kHz frequency band of the high frequency acceleration in the 15 to 35 kHz frequency band.

$\Sigma A_i N_i$: The $\Sigma A_i N_i$ where A_i is the value of the amplitude bin "i" in an acceleration histogram built on the acceleration sample values of the HP3562A spectrum analyzer and N_i is the number of recorded samples of amplitude A_i.

C.FACT: The acceleration crest factor (Peak to RMS ratio of the time signal) of the unfiltered accelerometer signal including its resonance.

Table 1 lists the correlation coefficients of the linear curve fits of the measured erosion rate to these parameters for a set of 28 test points where valid data existed for all parameters except the last one where only 26 test points were available.

Inferred Forces on the Profile. Prior to running the flow tests in the cavitation tunnel, the transmissibility function shown in Figure 7 expressing the ratio of the profile acceleration autospectrum to the input force autospectrum was measured. For this purpose a miniature high frequency impact hammer was utilized to excite the almost fully submerged profile in the neighborhood of the first five DECER probes and the response acceleration was recorded to produce a spatially averaged

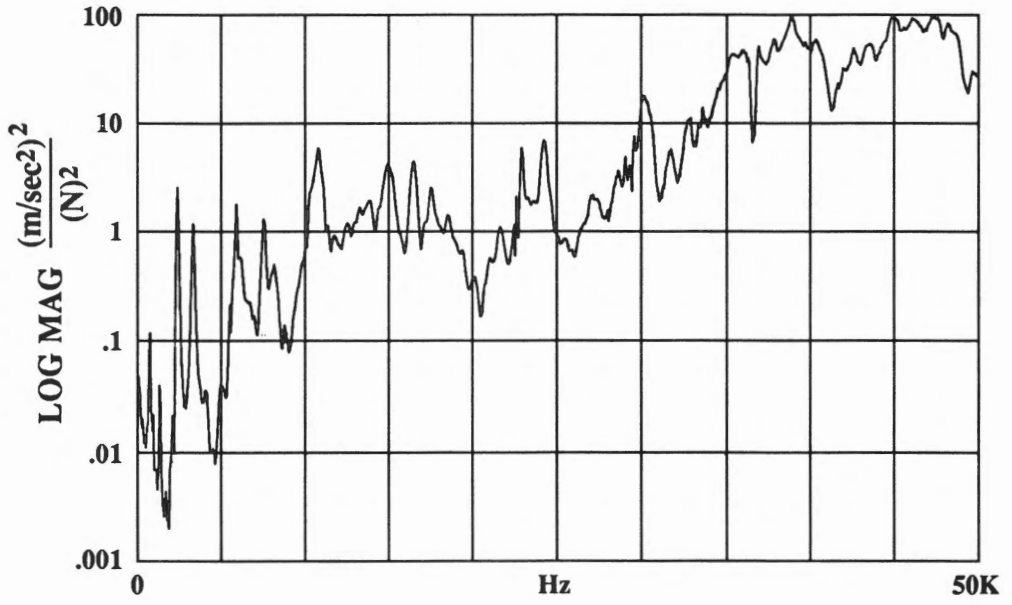

FIGURE 7 NACA 009 PROFILE TRANSMISSIBILITY FUNCTION

transmissibility function on a two channel FFT spectrum analyzer in the 0 to 50 kHz frequency range. With this function it is possible to recover the autospectrum of the acting forces on the profile by dividing the measured acceleration autospectrum at the monitoring point by the transmissibility function. Examination of these force spectra revealed that the main acting forces were confined to the 0-3 kHz frequency range where the impact frequencies were observed (Figure 4). The measured erosion rates in mm/a of titanium are shown in Figure 8 against the MSV of inferred forces in the 62.5 to 3000 Hz frequency band. These forces span the range of 100 to 600 000 N^2 which translates to an equivalent RMS span of 10 to 775 N.

Individual cavitation indentation marks left on the profile during the tests covered approximately areas of 1 mm^2. If we consider this area typical for the cavitation impacts, the equivalent localized acting impact stresses would vary between 10 to 775 MPa in a RMS sense. In the case of the most severe erosion recorded, the peak to RMS ratio of the response acceleration was observed to be 15. This suggests that peak localized impact stresses under these conditions could be as high as 775 MPa x 15 = 11625 MPa, well beyond the ultimate strength of the best alloys. Such high stresses cannot in reality take place because the local deformation of the material will cause a stretching of the attacked area with a corresponding limitation in the attainable peak stresses. Additionally, the hypothesis that the RMS forces act on a single 1 mm^2 area is a worst case situation. However, these inferred forces quantify the effective damaging potential of the imploding vortices.

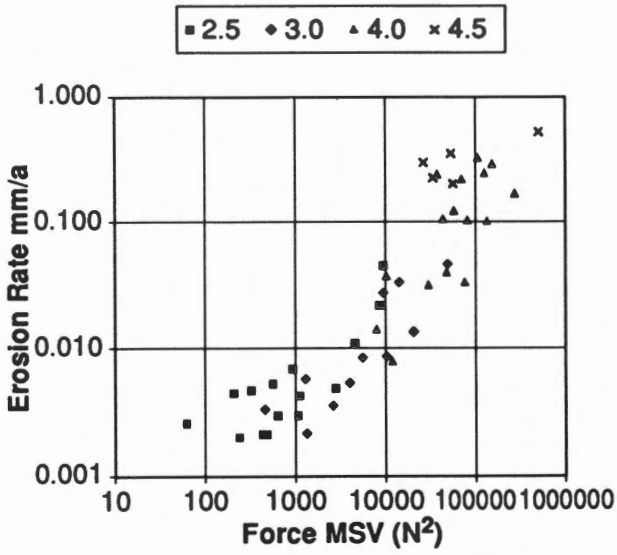

FIGURE 8 EROSION RATE VS THE MSV OF INFERRED FORCES ON THE PROFILE IN THE 62.5 TO 3000 HZ FREQUENCY BAND

Erosion and Acceleration Crest Factor. The impulsive character of the acceleration signal was very evident under erosive conditions. The peak to RMS ratio (Crest Factor) of the

TABLE 2
MSV OF ACCELERATION RATIO IN dB OF CASE B/CASE A

	Frequency band in kHz							
	2.5-15	16-22	23.5-31	31.5-46.5	47.5-62	63.5-77.5	79-93	94-100
B/A Ratio in dB	+1.57	+2.58	+5.92	+4.25	+3.43	+2.82	+4.86	+6.55

accelerometer signal dominated by its mounted resonance at ≈ 90 kHz was 5.0 and remained below 6.0 as long as the cavity length on the profile did not exceed 10 mm. The actual mounted resonance of the accelerometer was lower than the nominal catalog value of 125 kHz because of the thick glue line beneath the accelerometer. It was unusually thick because of the problems involved in mounting the accelerometer in a difficultly accessible location inside the profile tilting mechanism. The 90 kHz resonance thus produces ≈ 1dB amplification (+12%) of the true acceleration at 30 kHz. Higher frequencies can of course be used for measurement purposes on a relative basis as was done here at the accelerometer resonance inasmuch as the same frequency band is utilized throughout the test program for comparison purposes. Under these conditions, erosion levels on the profile were less than 0.005 mm/a, at or just above the detection threshold of the DECER probes. For erosion values of 0.02 mm/a and above, the crest factor was constantly above 12, varying between 12 and 25. Figure 9 shows that the crest factor for any given profile tilt angle tends to rise with increasing erosion rates up to a peak in this parameter. Then for the three higher blade tilt angles, there is a slight decrease in erosion with increasing crest factor. The explanation of this trend is not evident. The important information in this graph lies in the fact that low values were observed (< 6) when the visible leading edge cavity was very short (< 10 mm) or inexistent. Thus a crest factor of the order of 5 on a turbine prototype would suggest a very small likelihood of leading edge cavitation erosion. A higher crest factor would increase erosion risks.

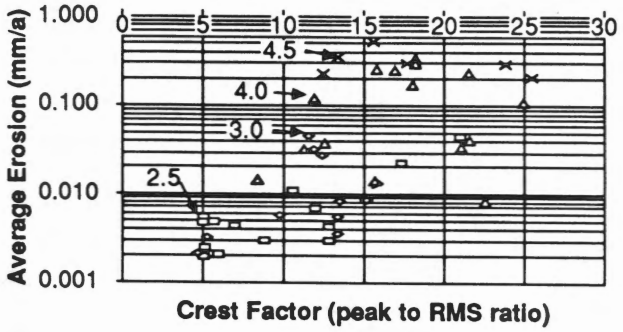

FIGURE 9 EROSION RATE VS ACCELERATION CREST FACTOR

The Signature of Erosive Cavitation. The appearance of a leading edge cavity triggers a wide band quantum increase in profile acceleration above approximately 2.5 kHz. An illustration of this can be found in Table 2 which lists the increases in the mean square value of the profile acceleration in frequency bands excluding spectrum analyzer basic noise components for two low level tests in the cavitation tunnel. Case A conditions were as follows: blade tilt angle, 2.5 degrees, water velocity, 35 m/sec, cavitation coefficient (sigma), 1.3, leading edge cavity length, 0 mm. Case B conditions were identical with the exception of the sigma value which was lower at 1.1. This change brought about a short leading edge cavity 8 mm in length.

This example shows that the increase in profile MSV of acceleration is substantial, particularly at the higher frequencies when a short leading edge cavity appears, all other conditions being equal. At lower velocities and sigma, incipient cavitation also triggered similar increases in acceleration above ≈ 2.5 kHz but the increase was concentrated in the lower 2.5 to 50 kHz range for this "softer" type of leading edge cavitation. As the cavitating flow becomes measurably erosive with the DECER probes, a crest factor well above 5 is observed in the high frequency acceleration signal. However the transition from non erosive cavitation to erosive cavitation is gradual and no radical change in vibratory signature is observed. The impulsive nature of the signal is very visible in the time domain and the impacting frequency is characterized by the Strouhal relation of Figure 4 which is linked to the main cavity pulsation frequency [1-2]. The Mean Square Value of high frequency acceleration increases linearly with the erosion rate as seen in Figure 6. From Figure 7, an inferred MSV of force of 10 000 N^2 or 100 N RMS is required to produce a measurable erosion rate of .02 mm/a of Titanium on the profile. The set of conditions mentioned above are required to ascertain the existence of an erosive leading edge cavitation condition. Acceleration measurements at high frequencies (15 to 35 kHz in the cavitation tunnel) can be utilized to characterize the relative erosion risk of a machine at different operating points but a characterization of the transmission path from the attacked areas to the response accelerometer is required for absolute indications, along with consideration for the material resistance to erosion.

The Erosive Power of Leading Edge Cavitation. The periodicity of the imploding vortices which impact the profile in the pressure recovery area at the closure region of the leading

edge cavity allows to develop the following expression for the mean erosive power [7-8] of the cavitating flow:

$$E = 1/2\ \rho\ F\ (C_p\ max + \sigma)\ v^3\ l^2\ [W]$$

This expression is derived from the potential energy of a single cavity collapse scaled on the leading edge cavity length and coupled to the Strouhal number governing the implosion frequency. F is a proportionality factor introduced to condense in one term the influence of σ and of the flow incidence. When the ratio of the corresponding inferred forces in the 15 to 30 kHz frequency range to the cavitation erosive power calculated with $1/2\ \rho_0\ v^3\ l^2$ is plotted against σ as shown in Figure 10 all the data tend to collapse into one curve even on a graph using linear axis scales. This non linear curve, built over all combinations of test conditions in the tunnel, illustrates the decreasing damaging efficiency of cavitation under very low sigma. This is due in part to the many cavities that do not implode on the profile but are lost in the flow downstream of the profile under these conditions. The continuity in this curve suggests that the forces acting on the profile under cavitating conditions are linked by a relatively simple relation to the potential erosive power of the flow as defined above thereby giving a rational hydrodynamic basis to a measured mechanical parameter. The notion of erosive power may therefore be a realistic and significant descriptor of the cavitation damage risk of a hydraulic machine and may become a useful tool in assessing prototype cavitation damage risks from model tests. After having identified the vibratory characteristics of erosive cavitation as indicated in the section on "Erosion and Acceleration Crest Factor" above and with the concept of erosive power of a cavitating flow defined, we turned our efforts toward identifying these parameters in the more complicated cases of model and prototype Francis runner.

MODEL AND PROTOTYPE FRANCIS RUNNER PROGRAM

Runner Selection

Cavitation Requirements. In order to meet the two main project objectives of establishing the equivalence of stationary and rotating sensor cavitation measurements and of identifying a vibratory cavitation pitting fingerprint, it was necessary to select firstly a prototype Francis runner with a known cavitation erosion history and secondly a prototype for which an homologous model existed and was available for testing. A runner which could fulfil these requirements at the time was a Francis runner (unit no 6) at the Hydro-Québec Rapide Blanc powerhouse on the upper St-Maurice river. This unit was a new replacement runner on its initial tour of duty. After 18134 hours of operation distributed as follows, 699 at 0-30%, 543 at 30-55%, 13669 at 55-75%, 1572 at 75-89.5% and 1697 at 89.5-100% guide vane opening, the machine was inspected and the cavitation damage was found to be light. Only 5 blades required welding repairs to replace an estimated volume of stainless steel of 84.5 cm^3 or 0.7 kg of lost material on the back of the blades. Minor repairs on the band accounted for 0.2 kg of additional stainless steel. Six other blades required surface polishing and slight repairs at the blade to band junction at the exit of the runner. The blade damage pattern is illustrated in Figure 11. A fully homologous model runner was available for testing at the G.E. Canada (DEW) Hydraulic Laboratory in Lachine, Québec.

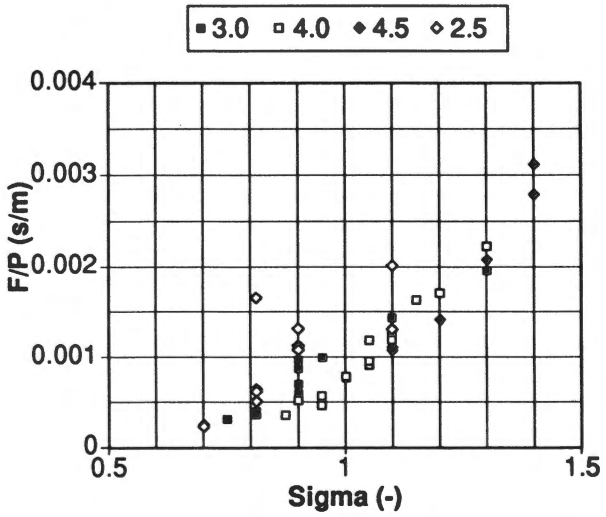

FIGURE 10 FORCE TO EROSIVE POWER RATIO VS σ

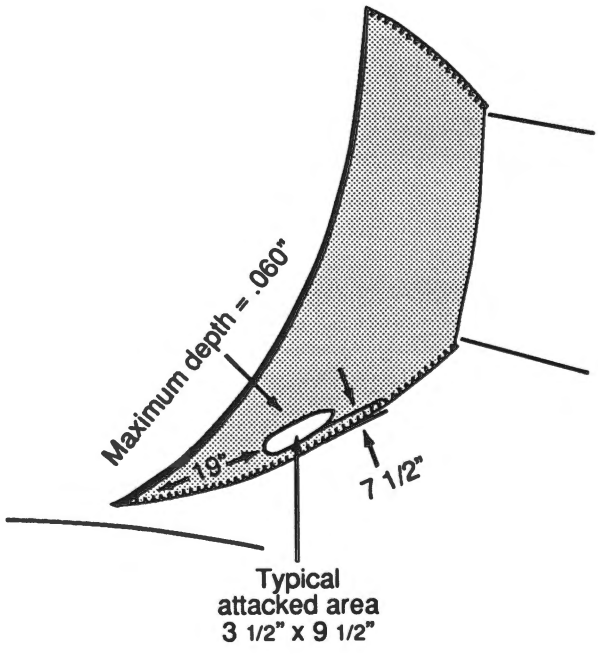

FIGURE 11 CAVITATION DAMAGE PATTERN ON RAPIDE BLANC PROTOTYPE

TABLE 3
PROTOTYPE AND MODEL CHARACTERISTICS

	Gross head m	R.P.M.	Sigma	Speed Coeff.	Blades	Guide Vanes	Stay Vanes	Draft Tube	Power at best effi.
Prototype	33.77	109.1	.24	.885	15	20	10	Moody	≈ 32 MW
Model	Net head 15.24	968	.24	.885	15	20	10	Moody	—

Prototype and Model Characteristics. The main characteristics of the prototype and model are summarized in Table 3.

Model Homology. The homology ratio between the prototype and the model was 13. The model was tested on G.E. Canada (DEW) test stand no 4. The runner, guide vanes and distributor height were fully homologous. The stay vanes were of very similar shape to the prototype stay vanes but their orientation was slightly different. The spiral case on the model was of the semi-spiral type as opposed to the full spiral on the prototype. The draft tube was of the Moody type as on the prototype with approximately the same scaled down depth but a slightly different width. These minor differences were not expected to affect the cavitation performance of the model according to G.E. Canada (DEW) engineers.

Instrumentation

Sensors. To meet the project objectives, two Kistler 8616A 1000 accelerometers were mounted radially in the crown of the model runner 180 degrees apart from each other in specially machined watertight compartments above blades 1 and 8 respectively. A third accelerometer of the same type was mounted radially on the lower guide hearing housing along with a Physical Acoustics Corporation WD wide band Acoustic Emission sensor. The signals from the rotating high frequency accelerometers were brought out to the stationary environment through a practically noiseless sealed mercury contact slip ring arrangement. A tachometer probe provided a once per revolution synchronisation signal for data acquisition. Additionally, the miniature impact hammer used on the profile was also used to measure transmissibility functions on the model along with a Wilcoxon ultrasonic exciter.

All hydraulic parameters such as flow rate, pressures, water temperature, and mechanical parameters such as r.p.m., torque and power output were measured with DEW test stand no 4 standard sensors. An endoscope was specially utilized to detect visually the presence of leading edge cavitation. High speed video recordings at 2000 pictures per second were made at three guide vane openings, still 35 mm stroboscopic photographs were shot for all test conditions and Fuji Prescale pressure sensitive film was utilized to confirm the damage model observed in the high speed cavitation tunnel.

The same accelerometer and Acoustic Emission sensor were used radially on the lower guide bearing of the prototype. A shaft mounted accelerometer with a wide band (30 Hz-30 kHz) FM transmitter were used to broadcast cavitation information to the stationary data acquisition system. The Wilcoxon ultrasonic exciter and a 50 000 pound force impact hammer were utilized to measure transmissibility functions on the prototype.

Data Acquisition Systems. For the model tests, the DEW test stand no 4 data acquisition system computed all the pertinent hydraulic and mechanical parameters. For the vibratory measurements on the model and the prototype, the data acquisition systems of Figure 2 less the DECER probes and acquisition system were utilized but with different filter frequencies and bandwidths and with the additional feature of synchronized data acquisition with the tachometric probe.

Transmissibility Function Measurements. As was done on the profile in the cavitation tunnel, the transmissibility functions linking the erosion damaged areas on the blades to the vibration monitoring point on the lower guide bearing housing were measured using impact techniques on both the model and the prototype. A verification of the principle of reciprocity was made on both the model and the prototype in air by also exciting the structures at the lower guide bearing and measuring the acceleration response on the back of the blades. It was found that reciprocity appeared to apply to both the model and the prototype [9]. On the model, at least, it was also found important to measure the transmissibility function with the model in water. It was therefore measured in water using the reciprocity approach with an accelerometer attached to a blade and impacts applied to the guide bearing housing with an impact hammer. The reverse was done in the dewatered prototype. The transmissibility functions thus measured, though not optimized, will allow to at least infer the order of magnitude of acting forces on both the model and the prototype.

Test Conditions

Model Tests. The model was tested at plant σ and prototype speed coefficient. Prototype equivalent guide vane openings of 41, 46, 57, 65, 78, 86, 92, 97 and 100% were explored.

Prototype Tests. The following sequence of test points was followed: 2, 50, 65.1, 75.1, 85.1, 95.1, 99.6, 95.0, 84.9, 65, 6, 85.1, 95.0, 99.4, 95.1, 85.1 and 9.1% guide vane opening. The initial run-up in power was followed by a rundown through most of the same points and after identifying the existence of a cavitation hysteresis loop above 85% guide vane opening, a second run around this loop was made for verification purposes. This hysteresis effect is illustrated in Table 4 which lists the MSV of acceleration in m^2/sec^4 observed at the lower guide bearing in the 15-30 kHz frequency band for both run-ups and rundowns around the hysteresis loop. The maximum values are recorded at 95% guide vane opening on the rundowns. The recorded values are repeatedly ≈ 2.5 times higher than those observed at the same guide vane openings on run-up. This hysteresis effect was more pronounced in the 70-85 kHz band where an amplification factor of 6 was recorded on rundown at the same guide vane opening.

TABLE 4
MSV OF ACCELERATION IN THE 15-30KHZ FREQUENCY BAND

	Guide Vane Opening		
	85%	95%	100%
1st Run-up	.258	.125	.167
1st Rundown	.234	.308	
2nd Run-up	.226	.105	.154
2nd Rundown	.244	.268	

Now that the structures of the model and prototype experimentation programs have been defined, we will now examine on a comparison basis the results obtained in both cases in relation also to the results of the high speed cavitation tunnel program.

MODEL/PROTOTYPE PROGRAM RESULTS

Model and Prototype Power Output

A preliminary step in comparing the cavitation performance of model and prototype runners consists in verifying that model and prototype behave similarly from a power point of view. This is confirmed in Figure 12 where the normalized mechanical power of the model is compared with the normalized electrical power generated by the prototype against guide vane opening. Each parameter is normalized to the maximum value measured experimentally for itself during the test sequences. Although the two parameters are not identical and the prototype electrical power is read off a meter with limited resolution the similarity of both curves indicate that model and prototype are consistent with each other.

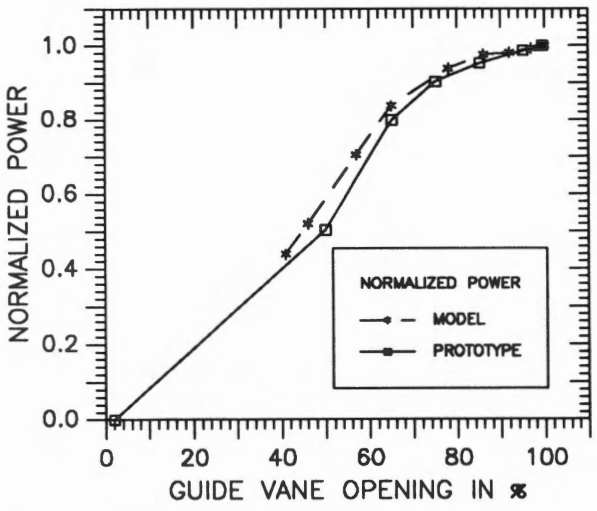

FIGURE 12 NORMALIZED POWER VS GUIDE VANE OPENING

Equivalence of stationary/Rotating Measurements

Model Runner. To evaluate the equivalence of stationary and rotating measurements, the MSV of acceleration in various frequency bands recorded by stationary and rotating accelerometers were correlated together. Although the frequency response of an accelerometer is not flat, particularly when the mounted resonance frequency is approached, once the accelerometer is mounted in a stable time invariant way, its amplitude response in a given bandwidth is linear within its mechanical/electrical dynamic range. Relative comparison of parameters in the same bandwidths are then possible to validate the existence of linear relationships between data measured at different locations on a structure. This is particularly useful in the case of cavitation studies where the short rise times of the cavitation impulses generate very high frequency components which can be more easily separated from other sources of low frequency noise. Figure 13 illustrates the similarity of the MSV of acceleration in the 70 to 85 kHz frequency band measured at the lower guide bearing and by the rotating accelerometer above blade 1 in the crown of the runner. The values on the curves for each sensor are normalized against the maximum value recorded for that sensor at its measurement location in the frequency bandwidth considered. The two curves at the bottom of the Figure were recorded with the plant sigma of .24 increased to 1.18 by pressurizing the downstream tailrace tank to extinguish all traces of cavitation on the model. Complete extinction was only achieved at 65° guide vane opening at best efficiency as intermittent hub vortex cavitation trails appeared at the three higher openings. These curves confirm the pertinence of the MSV of acceleration as a cavitation detector. The excellence of the linear correlation between the rotating and stationary measurements is illustrated in Table 5 which lists the values of the correlation coefficient of linear curve fits between the Mean Square Values of acceleration of both sensors measured in three

bandwidths. These coefficients were calculated with Lotus 123 software based on data measured simultaneously for both sensors and averaged over 150 8 msec time acquisitions on a 13 bit resolution high accuracy 2-channel frequency spectrum analyzer. The use of 150 averages results in a ≈ ± .5 dB statistical error band on power averages at the 90% confidence level. At least four significant digits for the data in each frequency band at each test point were retained for the curve fits. Within the constraints of the stability of the two measurement chains during the data acquisition for each test point, the three correlation coefficients all indicate an excellent linear relation between the stationary and rotating measurements with a slight possible increase in quality at the upper frequencies.

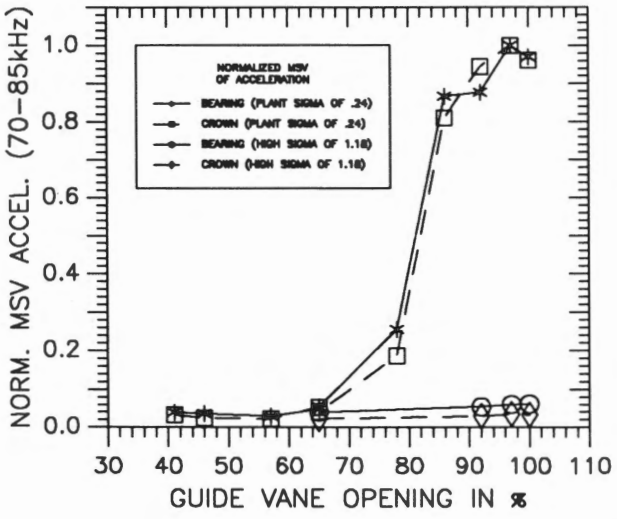

FIGURE 13 GUIDE BEARING AND ROTATING ACCELEROMETER P1 NORMALIZED MSV OF ACCELERATION VS GUIDE VANE OPENING

TABLE 5
FREQUENCY DOMAIN CORRELATION COEFFICIENTS

Parameter	M.S.V. of Acc. 15-30 kHz	M.S.V. of Acc. 15-30 kHz	M.S.V. of Acc. 15-30 kHz
Correlation coefficient	.9843	.9896	.9916

Very good correlations were also obtained at high frequencies with envelope detection and time domain parameters such as Peak values and signal standard deviation. The equivalence of stationary and rotating measurements was therefore clearly demonstrated on the model with stationary measurements performed exclusively at the lower guide bearing.

Prototype Runner. The equivalence of rotating and fixed measurements was also demonstrated on the prototype but the quality of the demonstration was hampered by a high threshold noise level in the FM transmitter whose sensitivity had been selected for higher levels of cavitation and also by its limited bandwidth. Individual cavitation peaks were visible simultaneously on both the shaft and guide bearing accelerometers and the same trends were observed above 65% guide vane opening when equivalent bandwidths of the signal from both sensors were compared. It can therefore be safely said that stationary cavitation measurements as proposed at the lower guide bearing of a Francis runner are equivalent to much more complicated measurements with on-board sensors and expensive transmission apparatus.

M.S.V. of Model and Prototype Acceleration

Measurements on the prototype revealed a much greater absolute increase above 50 kHz than below in the acceleration autospectrum level at the guide bearing for guide vane openings above the best efficiency point. This was also confirmed by the Acoustic Emission sensor operating in the .1 to 1 MHz frequency band. For this reason we have chosen to compare the MSV of acceleration in the 70 to 85 kHz frequency band at the lower guide bearing on both the model and prototype on Figure 14. We have also included data for the prototype in two lower frequency bands which behave in a different way. To avoid any problems in comparing, at high frequencies, on an absolute basis, data from two different sensor mounting configurations, here again we utilize data normalized against the maximum value measured in each bandwidth for each sensor. This allows to identify how model and prototype behave relatively from a cavitation point of view as a function of guide vane opening while avoiding completely the problems of accelerometer absolute accuracy at high frequencies. This figure suggests that model and prototype behave differently from a cavitation point of view. While both runners tend to peak at or near maximum guide vane opening when the 70-85 kHz band is considered, such is not the case at ≈ 95% where the relative performance of the two runners is in opposition. Here the model sees its maximum level while the prototype exhibits a significant dip in high frequency acceleration. If the cavitation performance of model and prototype were truly homologous, the same trends should hopefully be apparent in these curves and they are not above 80% guide vane opening. The prototype actually reached its peak acceleration value upon decreasing the guide vane opening from 100% to 95% after the run-up shown on the graph. At this operating point acceleration levels were twice as high as at full guide vane opening thereby revealing the existence of a significant cavitation hysteresis effect. This aspect could not be verified on the model because of test bench constraints making it difficult to maintain head while reducing guide vane openings. The prototype data in two lower frequency bands, 40-50 kHz and 15-30 kHz indicate different trends in the data with maximum values observed at lower guide vane openings. These frequency dependent differences were not apparent on the model where the same trends were observed in

all these frequency bands. This suggests that at least another high frequency noise source is present on the prototype, possibly flow noise due to surface roughness in the system or again to another form of cavitation associated with either larger imploding vapor structures or less steep recovery pressure gradients.

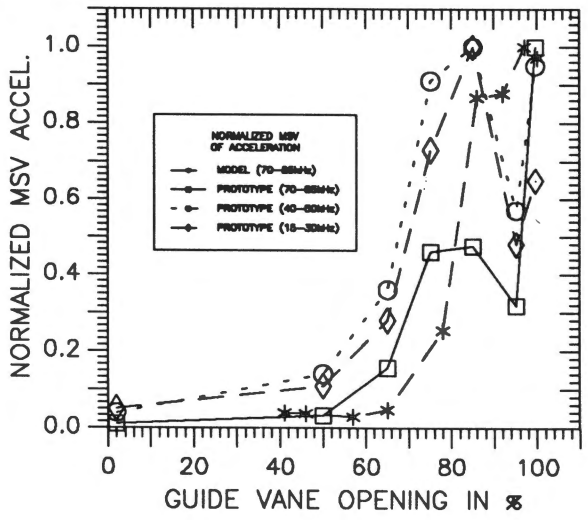

FIGURE 14 MSV OF GUIDE BEARING ACCELERATION NORMALIZED TO THE MAXIMUM IN EACH FREQUENCY BAND VS GUIDE VANE OPENING

M.S.V. of Inferred Forces on Model and Prototype

Forces resulting from cavitation attack on the blades of the model and the prototype were inferred with the transmissibility functions shown in Figure 15. Also shown are the coherence functions calculated for each transmissibility measurement ensemble. For the prototype, the transmissibility and coherence curves presented are the average values for blades 7 to 15 measured in air, each blade to guide bearing transmissibility being itself averaged 10 times. Blades 1 to 6 were excluded from the averaging process because one of the spectrum analyzer channels had been inadvertently left in DC coupling rather than AC during the data acquisition sequence. This deteriorated the coherence between the two measurement channels at the lower frequencies as the phase characteristics of both channels were no longer nominally identical. For the model, the data pertains to blade 1 only averaged 18 times in water, using a reciprocity technique as mentioned earlier. The coherence function indicates that the transmissibility data for the prototype can only be used with excellent reliability between ≈ 1.8 and 5.5 kHz and less so to ≈ 11 kHz. The corresponding data for the model is excellent from ≈ 1,5 to 20 kHz. Data outside of these frequency bands are not necessarily bad as low excitation forces at certain frequencies or the absence of response for certain modes at the response location will also cause low coherence at certain frequencies during transmissibility measurements.

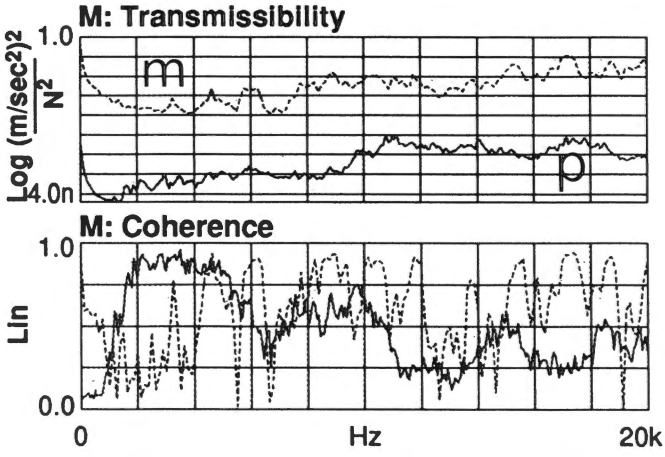

FIGURE 15 MODEL AND PROTOTYPE TRANSMISSIBILITY AND COHERENCE FUNCTIONS

The inferred force autospectra on the model and the prototype indicated that the major force components were located at frequencies below 10 kHz. Using the 0-10 kHz frequency band on the model and the 1-11,5 kHz band on the prototype, the maximum inferred per blade RMS force was 4 N on the model and 4300 N on the prototype. Thus model forces were lower than the minimum value of 10 observed on the NACA profile and the maximum prototype values were well above the 775 N maximum on the profile. Figure 16 shows the evolution of these inferred forces on the model and prototype with guide vane opening. The RMS values of the per blade inferred forces were normalized against the maximum value observed during the model run-up tests for the model and the maximum value observed for the prototype during the prototype initial run-up tests. If the cavitation performance of the model and the prototype are homologous, then we should expect the same type of leading edge cavitation development with the variation of guide vane opening. By normalizing the data as indicated above, the data in Figure 16 should illustrate whether the prototype follows the model trend in respect to inferred RMS forces. Since the data on these curves represent RMS values of force rather than Mean Square Values, the two curves differ by about 6 dB(100% in RMS terms, 400% in MSV terms) at low guide vane openings of ≈ 50%, by about 3.8 to 2.2 dB for intermediate guide vane openings of 65 to 85% and less than 1 dB (12% in RMS terms, 26% in MSV terms) at higher guide vane openings. The fine trends of the curves are also not identical as the monotonic increasing prototype curve does not show the three dips that are apparent on the model curve. These observations bring us to propose that here again, as apparent in Figure 14, the relative performances of model and prototype differ, but here on

the basis of forces that would be induced by cavitation. In order to get some insight in these differences the detailed cavitation signatures must be examined through time signal and amplitude modulation analysis in the frequency domain, in particular to see if the Strouhal relation observed in the cavitation tunnel is apparent in the vibration signals.

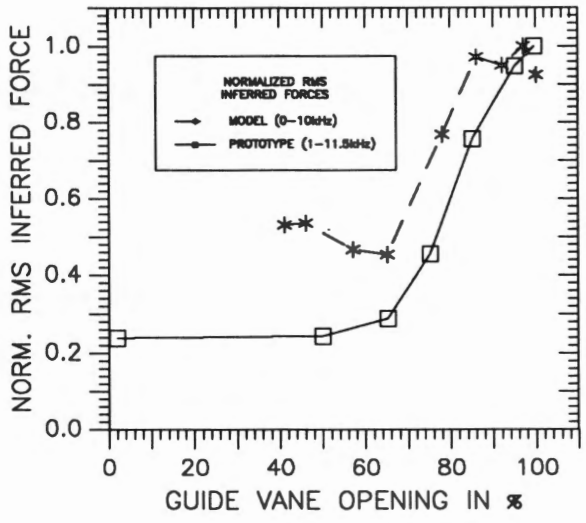

FIGURE 16 NORMALIZED RMS INFERRED FORCE VS GUIDE VANE OPENING

Impact rates on the model and the prototype

Strong impacts periodically spaced in time were visible in accelerometer time signals recorded on both the model and prototype. These are apparent in Figures 17 and 18 which show the strongest individual impacts on the model at 86% wicket gate opening and 99.6% on the prototype respectively. The Strouhal relation which characterized the impact rate in the cavitation tunnel was not observed in the model tests where leading edge cavity lengths were evaluated and correlated with the mid blade flow velocity. The theoretical impact frequencies were always lower than the observed impact frequency which appeared constant for all test conditions at the ≈ 15X (blade passing) frequency. On the prototype, a Strouhal relation could not be visually confirmed but there was no evidence of such a relation as in this case the 20X (guide vane passing frequency for a rotating observer) and/or its first harmonic at 40X determined the impact frequencies. The difference in time periods can be appreciated from Figures 17 (top to bottom: AE sensor, guide bearing accelerometer, crown accelerometers P1 and then P8) and 18 (top to bottom: shaft accelerometer and guide bearing accelerometer). High speed video film at 2000 pictures per second of the model revealed that a leading edge cavity grew from the blade to band junction and stretched longer and higher towards the crown on the back of the blade along the blade to band fillet as guide vane openings were increased. This cavity then detached itself from the blade to band junction and disappeared as it collapsed either on the back of the blades at the higher guide vane openings or in the flow between the blades at lower guide vane openings. On all visible blades this process was fairly well synchronised at the blade passing frequency but the synchronism was not perfect. A detailed examination of the individual major impacts visible in Figure 17 showed that each was composed of a cluster of ≈ 10 to 15 separate events happening within the blade passing period corresponding very probably to time scattered individual impacts on each blade with differential wave propagation times to the monitoring point.

The impact rates can also be estimated from frequency analysis of the amplitude envelope of high frequency acceleration observed at the guide bearing monitoring point. The technique of high frequency acceleration envelope analysis, an interesting and useful analysis tool, was originally proposed and utilized for cavitation studies by Abbot and colleagues [10,11]. It allows to identify high frequency signal amplitude modulation component frequencies and, in particular, when the impulsive character of the signal is established by time domain measurements, it can identify the average repetition rate of these impulses and their importance relative to the other modulation components present in the envelope signal. Analysis on the model was performed in the 70 to 85 kHz frequency band while on the prototype the 15 to 30 kHz frequency band was utilized. The relative amplitude of the significant high frequency acceleration amplitude modulation autospectra components for model and prototype are shown in Figures 19 and 20 respectively. In each figure, all modulation components are single frequency mean square acceleration components normalized against the maximum valued component observed for the tests performed at the guide vane openings identified on the "X" axis. For model data on Figure 19, this is the 15X component at 92% guide vane opening and for prototype data on Figure 20, this is the 20X component at 99.6% guide vane opening. The dominance of the 15X component on the model and of the 20X component on the prototype is evident. It is therefore clear that the impact frequency on both model and prototype does not follow the Strouhal law observed in the cavitation tunnel. The impact frequency on both runners appears governed by a hydrodynamic cavity growth and collapse mechanism associated with system flow characteristics which are not fully homologous between model and prototype.

The damage mechanism at the closure of the leading edge cavity was verified on the model with the use of Fuji pressure sensitive Prescale Film. After observing that the strongest impacts were recorded at 86% guide vane opening, strips of the film were mounted on each blade in the closure region of the stroboscopically observed leading edge cavities and the test point was repeated. The Fuji Low pressure grade of film developed saturated color on most of the blades (the water sealing tape failed on 4 of the blades) confirming the presence of high pressure impacts (≈ 1400 p.s.i.) in the closure region of the leading edge cavity. The shape and location of the pressure fingerprint was surprisingly similar to those of the damage pattern on the prototype (Figure 11). This result supports in a

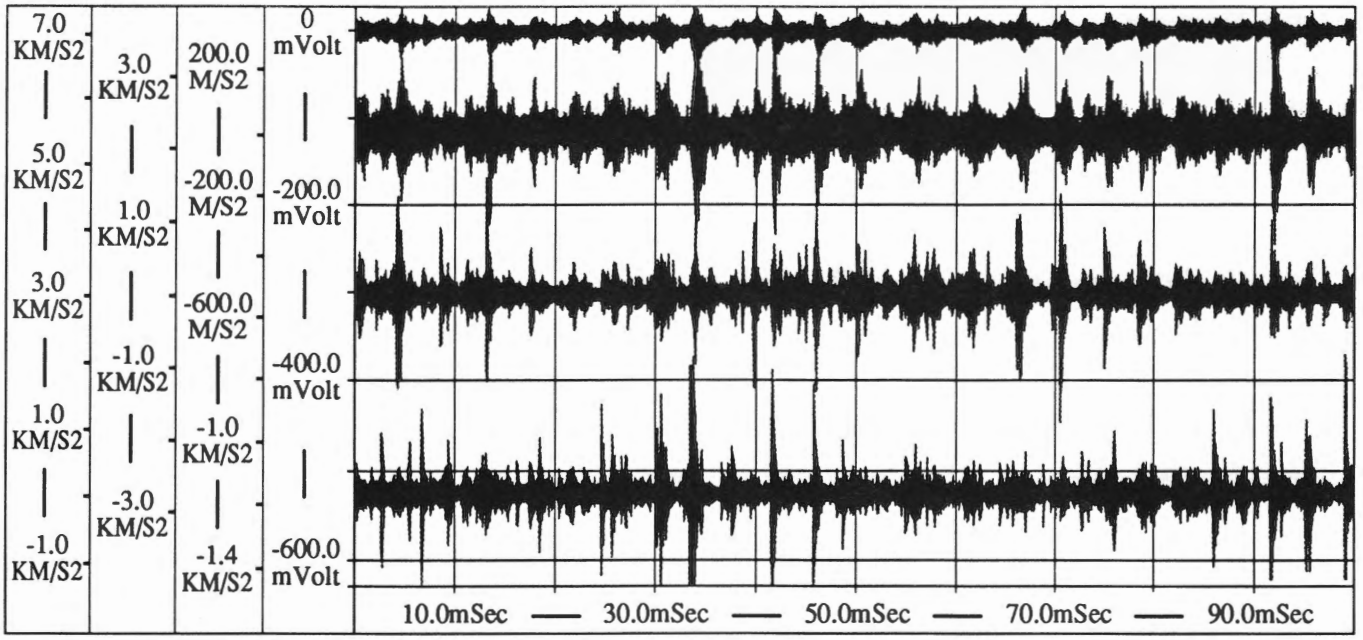

FIGURE 17 100 ms. TIME RESPONSE OF FOUR SENSORS ON MODEL AT 86% GUIDE VANE OPENING

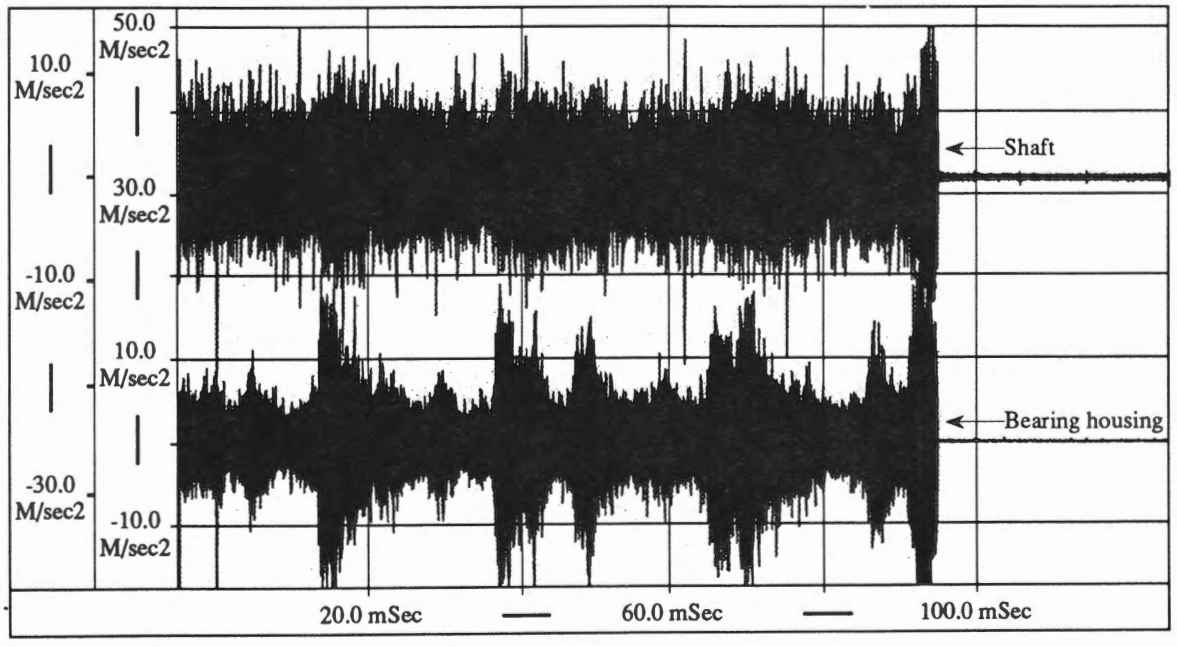

FIGURE 18 100 ms. HIGH PASS FILTERED SHAFT AND BEARING ACCELEROMETER SIGNALS AT 99.6% GUIDE VANE OPENING

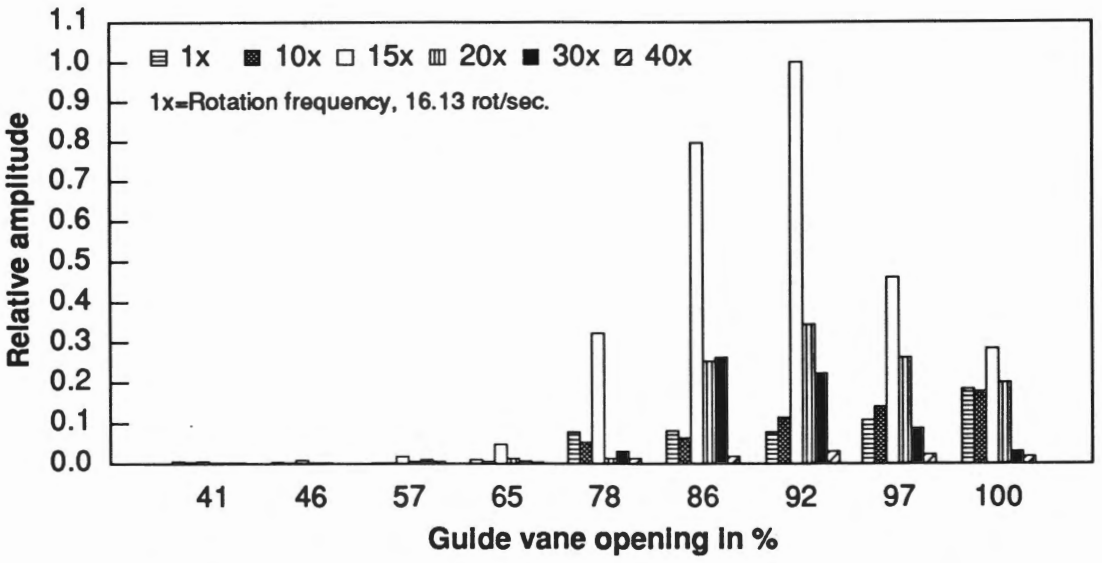

FIGURE 19 MODEL NORMALIZED HIGH FREQUENCY MODULATION COMPONENTS

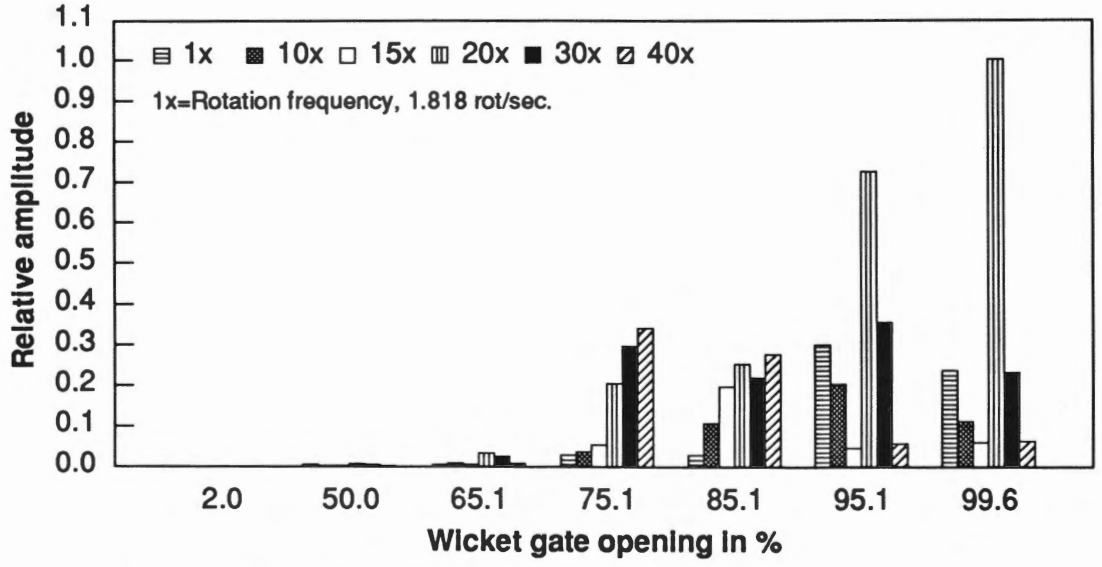

FIGURE 20 PROTOTYPE NORMALIZED HIGH FREQUENCY MODULATION COMPONENTS

very strong way the leading edge damage model established in the cavitation tunnel.

SUMMARY AND CONCLUSIONS

Equivalence of Stationary and Rotating Sensor Measurements

The equivalence of stationary and rotating vibratory measurements for the detection of cavitation was demonstrated on both the model and the prototype.

The Signature of Erosive Leading Edge Cavitation

Leading edge cavitation is the major cavitation damage source in Francis turbines. Controlled experimentation in the IMHEF high speed cavitation tunnel demonstrated that the transition to erosive cavitation is gradual and is simply a question of vortex impact intensities and material resistance to this attack. The impulsive character of the vibration signal is required along with high frequency content (> 2.5 kHz). The closure region of the leading edge cavities is the attacked area and RMS inferred forces greater than 100 N were found necessary to reach an erosion detection threshold of .01 mm/a of titanium. The impact rate on the profile was governed by a Strouhal law linked to the ratio of the flow velocity to the average cavity length. This relation gave rise to the notion of "erosive power" in the form of a V^3L^2 term where V is flow velocity and L is vapor cavity length.

Model Program

All of the above elements of an erosive cavitation signature were found on the model Francis runner with the exception of much lower inferred forces and the absence of the Strouhal relation. The Fuji Prescale Film confirmed the cavitation tunnel damage model.

Prototype Program

Here the only missing element is the Strouhal relation. Inferred forces higher than those of the tunnel were observed along with all of the other parameters. Actual cavitation damage was also present in the same areas identified by the Fuji film on the model.

Conclusions

Monitoring erosive cavitation through vibratory measurements appears possible but requires great care and objectivity as it is not a simple matter. The problems of differentiating erosive cavitation noise from non erosive cavitation noise or from turbulent flow noise which can all simultaneously occupy the same frequency spectrum are not yet solved. Also, other types of cavitation such as bubble cavitation may have different vibratory characteristics from those of leading edge cavitation. However, for absolute cavitation erosion measurements from vibratory signals, calibrated measurements including signal transmission path characteristics will be required. Also, another implicit element in such measurements which is not treated in this paper will be the consideration of the turbine material resistance to the cavitation attack as steel alloys with different cavitation erosion resistance will present the same types of cavitation vibratory signatures. However relative measurements can easily be made on runners if the cavitation impact signals can be separated from the flow noise. This appears possible at frequencies above 50 kHz. However calibration techniques on prototypes at these frequencies remain to be demonstrated. This stems from our experience with the prototype in this project where, in contrast to past measurements on other prototypes and on the model in this project, and as illustrated in Figure 14, the frequency content in various frequency bands did not vary in the same manner with guide vane opening. Lower frequencies could still be used when high frequency spectra behave uniformly in all frequency bands.

The notion of erosive power of a leading edge cavitating flow which fitted well with inferred forces on the profile as a hydrodynamic explanation for the measured mechanical results did not apply to the model or the prototype because the impact frequencies of the cavitating flow were not governed by the Strouhal relation observed in the cavitation tunnel. Instead, the impact frequency on the model was at the blade passing frequency whereas on the prototype it was at the guide vane passing frequency. However, if fully homologous model cavitation tests could be devised where both the cavity volume and the implosion frequency could be identified as a function of guide vane opening, then the potential erosive power of the model could be transposed to the prototype scale. Such homologous model cavitation tests should be confirmed by prototype tests and cavitation indications should correlate well with guide vane opening in both situations. Such was not the case in this project as the cavitation performance of the model and the prototype were not identical, differing in trends, in relative amplitude and most fundamentally in cavitation impact frequency. This last point suggests that the flow elements governing the cavity formation and collapse on the model and the prototype were different. These elements must therefore be considered if it is hoped to predict prototype cavitation performance from model tests. Additionally, in this process, the possible existence of a cavitation hysteretic behaviour of the runner must be examined.

ACKNOWLEDGEMENTS

The authors gratefully acknowledge the funding of this research project by the Canadian Electrical Association, Hydro-Québec and EPFL as well as the individual contributions of Pierre Lavigne of Hydro-Québec, Yan Kuhn de Chizelle and Mohamed Farhat of IMHEF who were highly instrumental in making the experimental programs and data processing and analysis a success.

REFERENCES

1 Avellan, F., Dupont, P., Ryhming, I., "Generation Mechanism and Dynamics of Cavitation Vortices

Downstream of a Fixed Leading Edge Cavity." *Proceedings of the 17th O.N.R. Symposium on Naval Hydrodynamics,* Session V, pp. 1-13, The Hague, The Netherlands, August 29 - September 2, 1988.

2 Avellan, F., Dupont, P., "Cavitation Erosion of Hydraulic Machines: Generation and Dynamics of Erosive Cavities.," *Proceedings of the IAHR Symposium, Trondheim*, p. 725-738, 1988.

3 Simoneau, R., Avellan, F., Kuhn de Chizelle, Y., "On Line Measurement of Cavitation Erosion Rate on a 2D NACA Profile," *Proceedings of the ASME International Symposium on Cavitation Noise and Erosion in Fluid Systems - 1989*, p. 95-102, San Francisco, 1989.

4 Simoneau, R. Bourdon, P., Désy, R., Grenier, R., "Cavitation Detection in Model Tests of Hydraulic Turbines," Phase 3 and Final Report, CEA report 230 G 439, May 1988.

5 Avellan, F., Henry, P., Rhyming, I., "A New High-Speed Cavitation Tunnel for Cavitation Studies in Hydraulic Machinery," *Proceedings of the ASME International Symposium on Cavitation Research Facilities and Techniques - 1987*, p. 49-60, Boston, Massachusetts, Dec, 13-18, 1987.

6 Simoneau, R., Bourdon, P., "Erosion and Impact Intensity of Vibratory, Jet and Turbine Cavitation," *Proceedings of the 16th Symposium of the IAHR*, Sao Paulo, Brazil, September 1992, pp. 627-636.

7 Bourdon, P., Simoneau, R., Avellan, F., Farhat, M., "Vibratory Characteristics of Erosive Cavitation Vortices Downstream of a Fixed Leading Edge Cavity," *Proceedings of the IAHR Symposium, Belgrade*, Vol. 1, paper H3, p. 1-12, 1990.

8 Avellan, F., Dupont, Ph., Farhat, M., "Cavitation Erosion Power," *Proceedings of the joint ASME-JSME Cavitation '91 Symposium*, p. 135-140, Portland, Oregon, June 23-27, 1991.

9 Bourdon, P., Simoneau, R., Avellan, F., "Hydraulic Turbine Cavitation Pitting Detection by Monitoring Runner Vibration," Draft Final CEA Report 307 G 657, December 1992.

10 Abbot, P.A., Gedney, C.J. and Brown, N.A., "Cavitation Monitoring of Two Axial-Flow Hydroturbine," *International Symposium on Cavitation and Multiphase Flow Noise*, 1986, ASME Winter Annual Meeting, Anaheim, CA, Dec.1986.

11 Abbot, P.A., "Cavitation Detection Measurements on Francis and Kaplan Hydroturbines," *International Symposium on Cavitation Noise and Erosion in Fluid Systems*, 1989, ASME Winter Annual Meeting, San Francisco, December 1989.